J. Hydrau., Coast. Environ. Eng., JSCE, No. 586/II-42, 127-135, 1998 February

WAVE AND CURRENT FIELDS AROUND GAPPED SUBMERGED BREAKWATERS

Eric C. CRUZ[1] and Toshio AONO[2]

[1]Dr. Eng., Research Engineer, Numerical Analysis Laboratory, Technical Research Institute, Toa Corporation (1-3 Anzen-cho, Tsurumi-ku, Yokohama 230, Japan <e_cruz@toa-corp.co.jp>)
[2]Member of JSCE, Dr. Eng., Chief, Numerical Analysis Laboratory, Technical Research Institute, Toa Corporation

The basic characteristics of the wave and current fields around gapped submerged breakwaters are studied by applying a nonlinear dispersive model for horizontally two-dimensional wave evolution on uneven bottom overlain by a porous layer. Verification of the model with wave basin experiments is presented. Simulations under an open sea condition reveal the wave height extrema on the crown and behind the gap. Currents are magnified around the crown corners on the seaward side. The effects of porosity on these characteristics are discussed.

Key Words: *submerged breakwater, breakwater gap, porous layer, wave field, currents, mean water level, extended Boussinesq equations*

1. INTRODUCTION

Submerged breakwaters are increasingly being used in coastal engineering works as wave protection and beach control device. Although their effectiveness is limited by the fact that they allow transmission into the shoreward region, the functional merits of crown submergence are often weightier to justify their adoption. These merits can be given as follows: (1) Submergence of the crown causes only partial wave reflection which is desirable if maritime vessels approach the enclosed area, as in a harbor. (2) Submergence induces breaking of waves on the seaward face, resulting in early dissipation of wave energy. (3) The rise of mean water level behind the structure is reduced. (4) A large amount of incident energy is transferred to higher harmonics[1] which generally cause less problems when harbor seiching is considered. (5) Submerged breakwaters are effective in modifying the scouring patterns of a sandy beach[2].

Porous structures are used for protection in harbors, inlets and beaches. They are also utilized as wave absorbers in wave tanks. Porosity provides effective damping action over a wide range of wave conditions. In fact, under suitable conditions (with no wave breaking), the incident wave energy can be dissipated significantly by porous damping alone.

Crown submergence and porosity generally induce opposing hydrodynamic effects. For example, wave shoaling on the seaward slope leads to an increase in wave height but porous damping may become dominant at a certain depth consequently arresting this height increase. Another example is wave set-up. Submerged structures induce offshore-bound currents which are sustained by mean water level increases, or wave set-ups, behind them. Due to porosity, there is additional space for the water to flow out, resulting in smaller wave set-ups in the shoreward side.

Previous studies of submerged breakwaters have dealt mostly with characteristic indices such as reflection, dissipation and transmission coefficients. Results have been reported for rectangular section on horizontal bottom based on experimental data[1], field data[3] and theoretical approach[1),4),5),6),7)]. A crucial step in studying porous media flow is the development of the porous resistance equation. Ward[8] was the first to propose an equation based on experimental results using various porous materials, which is applicable to both laminar and turbulent flow. It is recognized that the porous resistance equation for the unsteady wave motion should include the effect of local acceleration. This inertial effect was first incorporated by Sollitt and Cross[5] into a Forchheimer-type equation through the

added-mass concept. Gu and Wang[10] reported that the added mass coefficient determined experimentally for gravel sizes up to 3.74 cm is about 0.46 and not null as usually assumed. Sawaragi and Deguchi[9] have shown that the turbulent drag coefficient and permeability in Forchheimer resistance equation for oscillatory flow are different from those for steady flow. They proposed an empirically equivalent linear drag coefficient based on results of unsteady permeability tests.

Under a general combination of wave conditions, porous media properties and topography, none of these approaches, however, is applicable in analyzing the wave field. Mathematical modelling is generally used in such cases. Rojanakamthorn et al.[11] proposed an elliptic equation for horizontally two-dimensional linear wave transformation on porous beds which reduces to the mild-slope equation if the porosity becomes unity. For wave transformation in the vertical plane, a number of numerical models have been reported. Among these are models that used the finite difference method to study nonlinear wave interaction with a permeable surface breakwater[12], the finite element method to study internal flow in rubble-mound structures[13], and boundary integral equation method to study energy dissipation within porous submerged breakwaters[14]. Vertically-integrated equations have also been used to model one-dimensional wave transformation on porous bottoms using Boussinesq-type equations[15, 16] and coupled long wave equations[17].

Submerged breakwaters are usually constructed with fixed openings, creating regular, intermittent or isolated gaps along the structure. Gaps function, for example, as navigation entranceways, tidal outlets or as a means to improve circulation in an otherwise enclosed region. On account of the gaps, wave motion is strictly three-dimensional. In addition to the overflow on the crown and throughflow across the porous body, there will be refraction on the structure and diffraction around the corners. The gap also induces part of the incoming wave to be scattered offshore while the wave components that propagate shoreward undergo various degrees of porous damping through the breakwater. These processes will affect the horizontal distribution of wave energies around the structure as well as the currents that would exist if the breakwater were otherwise continuous.

The characteristics of the wave field are important in the design of the breakwater tip protection works while the currents are important in assessing maritime accessibility to the protected zone.

This paper aims to identify the basic characteristics of the wave field around such gaps or openings by applying a nonlinear dispersive model of horizontally two-dimensional wave evolution on a submerged structure that takes its porosity into account.

The applicability of the model is first shown through comparison with results of laboratory experiments. Then it is used to simulate the wave and velocity fields under an open sea boundary condition.

2. MATHEMATICAL MODEL

(1) Wave evolution equations

Boussinesq equations have been derived to model wave transformation on porous beds[18]. These are written:

$$\eta_t + \nabla\cdot[(h+\eta)\mathbf{u}] + \lambda\nabla\cdot(h_s\mathbf{u}_s) = 0 \tag{1}$$

$$\begin{aligned}&\mathbf{u}_t + \mathbf{u}\cdot\nabla\mathbf{u} + g\nabla\eta + \frac{h^2}{6}\nabla(\nabla\cdot\mathbf{u}_t)\\&-\lambda\frac{h}{2}\nabla[\nabla\cdot(h_s\mathbf{u}_{st})] - \left(\frac{1}{2}+\gamma\right)h\nabla(h\nabla\cdot\mathbf{u}_t)\\&-\gamma g h\nabla\left[\nabla\cdot(h\nabla\eta)\right] + \varepsilon\mathbf{u} = 0\end{aligned} \tag{2}$$

$$\begin{aligned}&C_r(\mathbf{u}_{st} + \mathbf{u}_s\cdot\nabla\mathbf{u}_s) + g\nabla\eta + \alpha\mathbf{u}_s\\&+\left(C_r\frac{\partial}{\partial t}+\alpha\right)\left[-\frac{h_s^2}{3}\nabla(\nabla\cdot\mathbf{u}_s) - \frac{h_s}{2}\nabla(\nabla h_b\cdot\mathbf{u}_s)\right.\\&\left.+\frac{h_s}{2}\nabla(h-h_s)\nabla\cdot\mathbf{u}_s + \nabla h\nabla h_b\cdot\mathbf{u}_s\right]\\&-\frac{1}{2}\nabla[\nabla\cdot(h^2\mathbf{u}_t)] - (1+\beta)\lambda\nabla[h\nabla\cdot(h_s\mathbf{u}_{st})]\\&-\lambda\frac{\beta g}{C_r}\nabla[h\nabla\cdot(h_s\nabla\eta)] - \lambda\frac{\beta\alpha}{C_r}\nabla[h\nabla\cdot(h_s\mathbf{u}_s)] = 0\end{aligned} \tag{3}$$

where η denotes the water surface displacement from still water level, $\mathbf{u}\equiv(u,v)$ and $\mathbf{u}_s\equiv(u_s,v_s)$ the depth-averaged horizontal velocity vectors in the free water and porous layers of thicknesses h and h_s, respectively, $h_b\equiv h+h_s$ the water depth on the impermeable bottom, g the gravity acceleration, x and y the horizontal coordinates and t the time. Subscript t denotes differentiation with time while the gradient operator is $\nabla\equiv(\partial/\partial x,\partial/\partial y)$. λ denotes the volumetric porosity which is assumed uniform and isotropic. γ and β respectively denote the celerity and porous damping extension factors that effectively extend the validity of Eqs.(1)-(3) up to the deepwater limit. With $\gamma=1/18$ and $\beta=1/15$, Eqs.(1)-(3) can be used up to $h/L_0=0.5$ and $h_s/h=5$ (L_0 is the deepwater wavelength).

C_r is the inertial coefficient defined as

$$C_r \equiv \lambda + (1-\lambda)(1+c_m) \tag{4}$$

where c_m is the added mass coefficient. The porous resistance consists of a linear (laminar) term and a nonlinear one:

$$\alpha \mathbf{u}_s \equiv (\alpha_1 + \alpha_2 |\mathbf{u}_s|)\mathbf{u}_s \tag{5}$$

where α_1 and α_2 are porous media coefficients that depend on the porosity, viscosity, permeability as well as on the shape and size of the porous medium. The total porous resistance actually consists of non-inertial effects represented by the right side of Eq.(5) and the local acceleration effect already included in C_r.

Eqs.(1)-(3) contain the leading order of wave nonlinearity and an extended range of dispersivity. Nonlinearity effects have to be considered because of the shallow crown where the relative wave height H/h can be significant. Dispersivity is necessary in order to reproduce correctly the wave celerity for a wide range of relative water depths. Dispersivity is also extremely important in depth-refraction and diffraction phenomena which are sensitive to gradients in local celerities.

In the absence of the porous layer, Eqs.(1) and (2) are used without the terms containing $\mathbf{u}_s$.

(2) Numerical implementation

The finite difference method is used to discretize Eqs.(1)-(3). An alternating-direction implicit (ADI) approach with a Crank-Nicholson scheme is used to reduce these to algebraic equations along the x and y directions in the unknowns η, $\mathbf{u}$ and $\mathbf{u}_s$. Along the x direction, η, u and u_s are first solved together for one half-time step, then η, v and v_s are solved together for the next half-time step in alternate fashion. In this way, the solutions are obtained without the need of iteration within each step.

The variables are recorded when their respective amplitudes have steadied. Attainment of this condition depends on the size of the computation domain, the incident wave parameters and the degree of discretization. In the computations reported here, a minimum run time of 25 wave cycles was used to allow the leading crest of the wave train to travel a distance of five times the domain length in the direction of propagation. Time and space discretizations were $T_{in}/60$ and $L_{in}/30$, respectively, where T_{in} and L_{in} denote the incident wave period and wavelength.

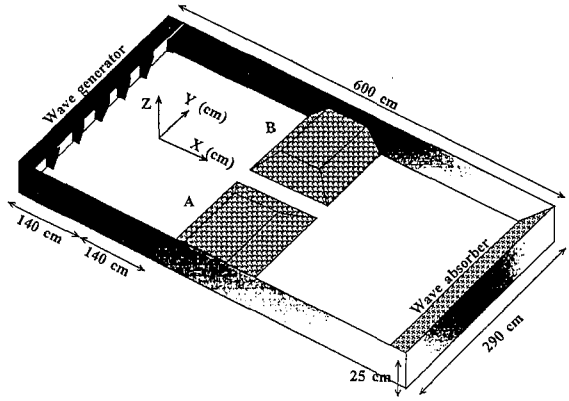

Fig.1 Wave basin experiment set-up and coordinate system

3. SIMULATION OF WAVE BASIN EXPERIMENTS

Regular wave experiments were conducted on a 6.0 m by 2.9 m by 0.25 m wave basin at the University of Tokyo (**Fig.1**). A physical model of a gapped porous breakwater was placed on the horizontal floor by constructing two identical gravel mounds A and B. The mound cross-section was trapezoidal with side slopes of 1:2 (vertical:horizontal) on all sides, with a rectangular crown measuring 52 cm by 108 cm. To allow the waves to propagate without breaking, the height of breakwater from the bottom was set at 8 cm and the water depth fixed at h_b=14 cm. The gravel used has mean diameter of 0.6 cm.

Incident waves were generated by a flap-type wave generator at x =-140 cm. At the other end, a wiremesh screen was placed to absorb the outgoing waves. To measure water surface displacements, a linear array of eight capacitance-type wave gauges spaced at 20 cm was set-up in front of mound A and moved at 20 cm intervals along x. A total of 136 gauging points was obtained and by assuming that the wave field is symmetrical about the centerline, the wave height distribution in the entire wave basin is determined experimentally. The incident wave height was determined by installing two resolution gauges along the centerline spaced at 30 cm and using the two-point method of Goda and Suzuki[19] to resolve the incident and reflected waves.

The distribution of measured wave heights, normalized by H_{in}, for one non-breaking case is shown in **Fig.2**. The incident wave height H_{in} is 1.48 cm

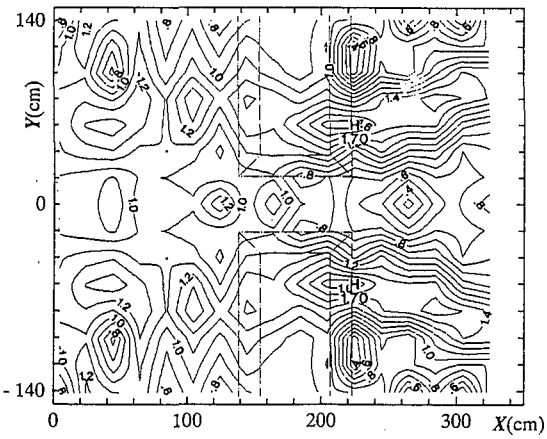

Fig.2 Measured contours of normalized wave heights H/H_{in} in wave basin experiments

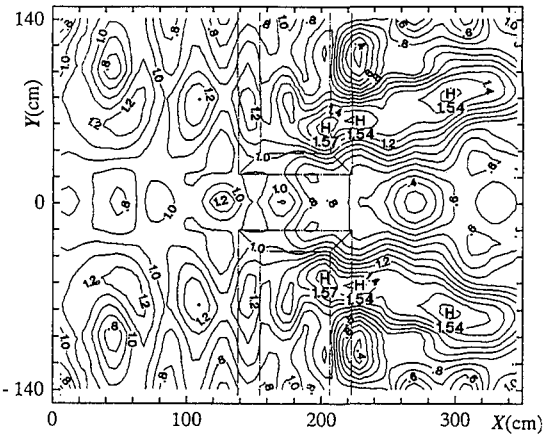

Fig. 3 Computed wave heights H/H_{in} in wave basin experiments

and the wave period is 0.82 s. H_{in}/h is 0.247 on the crown and the maximum h/L_0 is 0.133.

In the simulation, the porous resistance coefficients in Eq.(5) were determined using the equation of Sollitt and Cross[5], based on experimental results employing gravel material:

$$\alpha_1 = \frac{\nu\lambda}{K} \tag{6}$$

$$\alpha_2 = \frac{C_f\lambda^2}{\sqrt{K}} \tag{7}$$

where ν is the kinematic viscosity, K the intrinsic permeability, and C_f the turbulent friction coefficient. K and C_f are functions of the equivalent sphere diameter d of the porous material, up to d=3.5 cm. From their tabulated values and the gravel mean diameter, the following values were linearly interpolated: K =1.0×10^{-4} cm^2, C_f =0.428. Porosity λ=0.44 was determined from weight-volume relationships. Viscosity was taken as ν =1.0×10^{-2} cm^2/s. In the absence of available methods of determining the added mass of randomly packed granular material, c_m was taken as null.

Boundary conditions are specified at all sides of the basin. At the wave generator end x=-140 cm, the reflective conditions at the wave paddle are prescribed as

$$\frac{\partial(\eta-\eta_{in})}{\partial x} = 0 \tag{8}$$

$$\frac{\partial(u-u_{in})}{\partial x} = 0 \tag{9}$$

where η_{in} is the water surface displacement as given by the second-order Stokes wave theory (H_{in}/gT_{in}^2=0.0022, h_b/gT_{in}^2=0.021) corresponding to the incident wave height and period. u_{in} is obtained by integrating and averaging the corresponding depth-dependent horizontal velocity. Thus, the second-order bound harmonic, which is especially important on the shallow crown, is retained in both η and u.

Perfect reflection at the side walls is enforced by

$$\frac{\partial\eta}{\partial y} = 0 \tag{10}$$

$$\frac{\partial u}{\partial y} = \frac{\partial u_s}{\partial y} = 0 \tag{11}$$

$$v = v_s = 0 \tag{12}$$

at $y=\pm y_D/2$, y_D being the basin width. Eqs.(10) to (12) are valid for an actual side wall or an imaginary wall representing the boundary of the repeating section of a long breakwater with regular gaps.

The other end of the basin is taken as an open boundary since outgoing waves are assumed to be completely absorbed by the wiremesh screen. This is enforced by attaching a transverse strip of numerical wave absorber at the right end and applying Sommerfeld radiation condition at its outer edge:

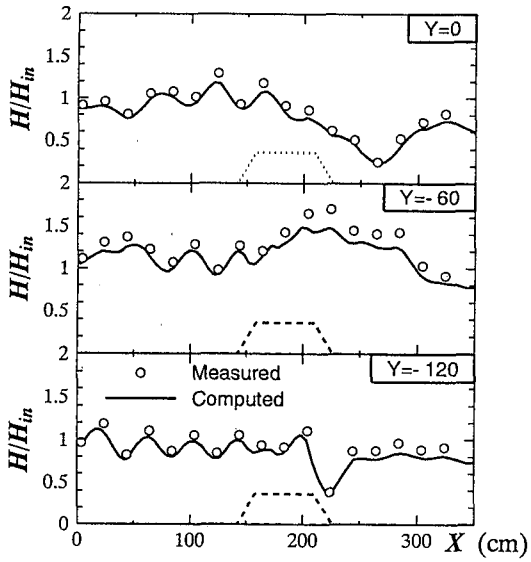

Fig.4 Longitudinal distribution of wave heights

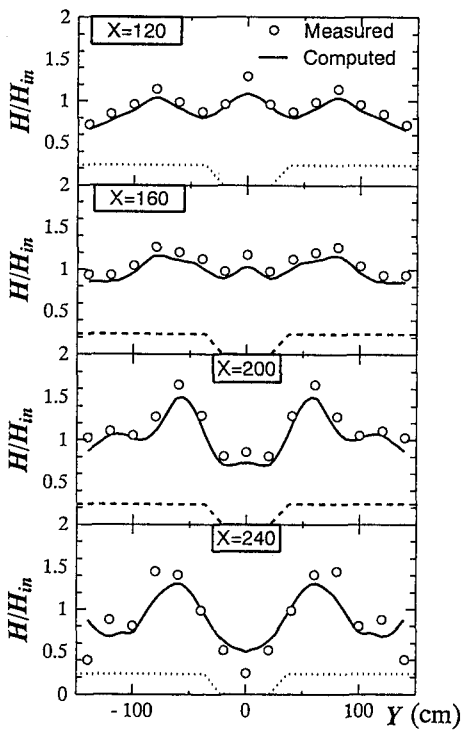

Fig.5 Transverse distribution of wave heights

$$\frac{\partial \eta}{\partial t} + C_s \frac{\partial \eta}{\partial x} = 0 \qquad (13)$$

$$\frac{\partial u}{\partial t} + C_s \frac{\partial u}{\partial x} = 0 \qquad (14)$$

at $x=x_D$, where x_D is the location of the outer edge. The wave celerity C_s is prescribed as the frequency-independent long wave celerity $\sqrt{gh_b}$. Within the absorber, the boundary damping function $\varepsilon(x,y)$ in Eq.(2) is uniform along y and linearly varies along x, while ε is null elsewhere. The properties of the absorber were determined from the simulation aid graphs in Cruz and Isobe[21] such that for a maximum reflection of three percent and damping width of $10h_b$, the range of absorbable frequencies is $h/L_0 = 0.04 \sim 0.50$.

The explicit conditions

$$v_s = 0 \qquad u_s = 0 \qquad (15)$$

are prescribed at all nodes where $h_s=0$ in order to solve for the velocities in the water and porous layers simultaneously through Eqs.(2) and (3).

Fig.3 shows the computed normalized wave heights in the vicinity of the gap. Compared with **Fig.2**, it is seen that the gross features of the wave field are well reproduced by the simulation. Partial standing waves exist in front of the mounds and the walls on the wave generator side. The gap causes a local concentration of wave energies in front of the seaward corners of the mound partly on account of oblique waves reflected from the gap and partly due to the rereflected waves. Longitudinal and transverse distributions of H/H_{in} are shown in **Figs.4** and **5**, respectively. Along the centerline, the wave height decreases along the gap to a minimum of about $0.28H_{in}$ behind it (**Fig.4**), mainly as a result of diffraction around the gap. At the shore side, local wave height extrema are observed. These extrema are caused by the interaction of the wave transmitted over and through the mound and the waves reflected from the walls. The transmitted wave has undergone various degrees of refraction and damping through the porous mounds resulting in the complicated patterns shown. On the crown, these patterns are nonexistent. We observe, however, the existence of a local high wave along the backface near the shoreward corners. The computation reproduces this feature although it slightly underestimates its value.

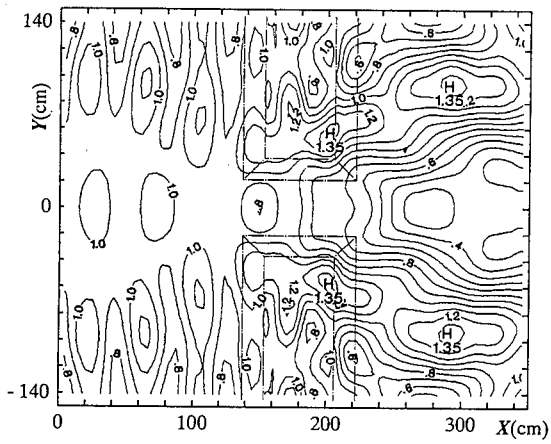

Fig.6 Computed wave heights *H/Hin*, porous submerged breakwater, open sea boundary conditions

4. GAPPED POROUS BREAKWATER IN OPEN SEA

In the open sea, waves reflected from structures propagate out into the far field without coming back. To simulate this condition, an offshore wave absorber is attached at $x=0$ across the basin width. The location of the offshore boundary is immaterial in this case since the boundary is virtually transparent to the outgoing waves. The damping distribution and absorber properties are identical to those of the onshore absorber. At the outer edge, the following boundary conditions are used:

$$\frac{\partial(\eta-\eta_{in})}{\partial t}-C_s\frac{\partial(\eta-\eta_{in})}{\partial x}=0 \qquad (16)$$

$$\frac{\partial(u-u_{in})}{\partial t}-C_s\frac{\partial(u-u_{in})}{\partial x}=0 \qquad (17)$$

Just like Eqs.(13) and (14), these boundary conditions are linear. The wave field at the outer zone of the boundary damping regions can be safely assumed to satisfy these conditions since the properties of the absorbers are optimally determined to suitably damp the outgoing wave.

The resulting wave field is shown in **Fig.6**. The wave heights throughout the basin are smaller compared to those in **Fig.3**. The seaward region is now dominated by waves normally reflected from the transverse faces of the mounds interacting with the oblique waves from the gap. The maximum wave height still occurs near the shoreward corners on the crown but is now smaller. The local minimum

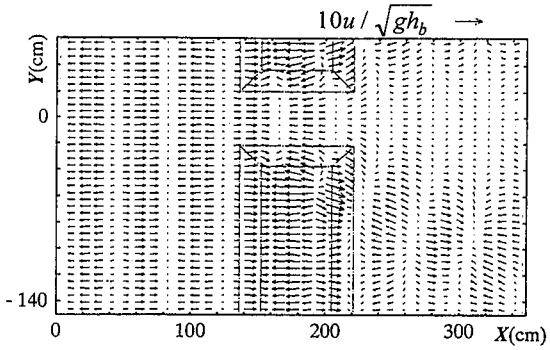

Fig.7 Normalized exterior depth-averaged velocities at $t=25T_{in}$, porous submerged breakwater, open sea boundary conditions

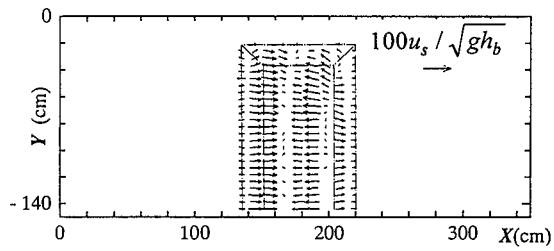

Fig.8 Normalized interior depth-averaged velocities at $t=25T_{in}$, porous submerged breakwater, open sea boundary conditions.

height still occurs behind the gap where diffraction is dominant.

Fig.7 shows the exterior velocities at $t=25T_{in}$ and **Fig.8** shows the interior velocities at the same instance. Exterior velocities are normalized by $0.10\sqrt{gh_b}$ and the interior velocities by $0.01\sqrt{gh_b}$. We can see that interior velocities are about an order of magnitude smaller than those in free water. **u** and $\mathbf{u}_s$ have a small phase lag indicating that a return flow occurs through the porous mound. Exterior velocities tend to be high near the seaward corner on the mound while high interior velocities are found within the crown where the relatively thicker porous layer can sustain them.

Fig.9 shows the computed currents outside the mounds obtained by taking the time-averaged velocities after the amplitudes have steadied. The maximum currents appear on the seaward corner on the crown. This is where u and v are largest due to flow convection resulting from large gradients in depths.

Fig.10 shows the distribution of mean water level normalized by H_{in}. Mean water levels behind the breakwater and near the walls have risen. On the contrary, those on the mounds and in front of the gap have gone down. It should be noted, however,

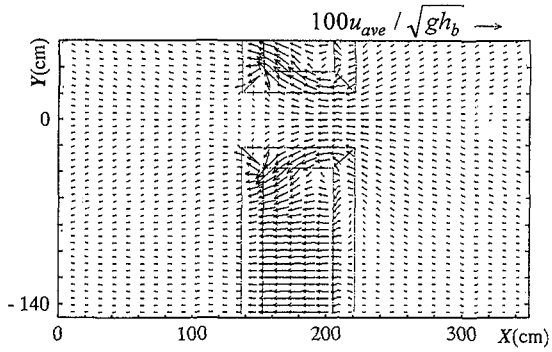

Fig.9 Normalized exterior currents, porous submerged breakwater, open sea boundary conditions

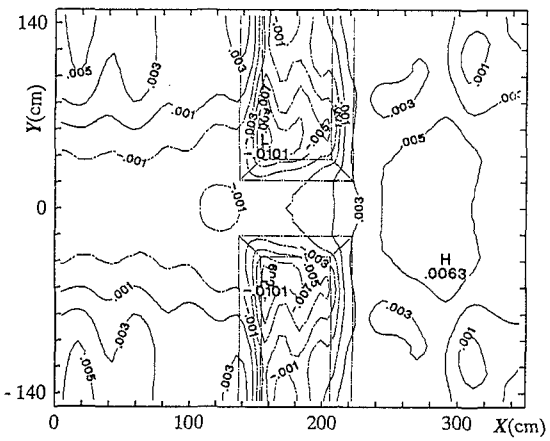

Fig.10 Normalized mean water levels, porous submerged breakwater, open sea boundary conditions.

that the numerical values of mean water levels are very small, of the order of $0.01H_{in}$.

Fig.11 shows two instances of the water surface displacements. Note that the long-crestedness of the incident wave breaks down as the crest encounters the gap while the portion nearer the wall undergoes attenuation through porous dissipation.

5. GAPPED IMPERMEABLE BREAKWATER IN OPEN SEA

To isolate the effects of porosity, simulation was carried out for an impermeable breakwater where the mound surface acts as the seabed. Only Eqs.(1) and (2) need to be solved and the porous media parameters become irrelevant. **Fig.12** shows the resulting wave field for such an impermeable breakwater under an open sea condition. Comparing

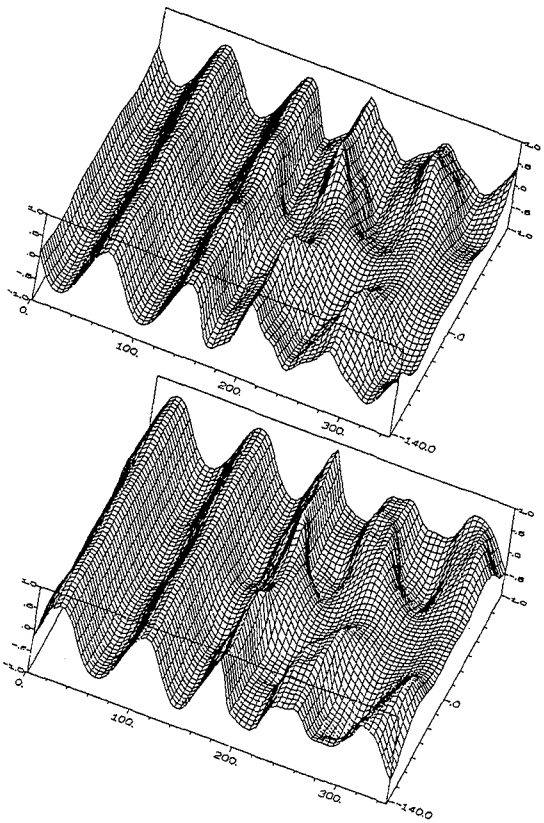

Fig.11 Normalized water surface displacements at $t=25T_{in}$ (top) and $t=25.50T_{in}$ (bottom), porous submerged breakwater, open sea boundary conditions

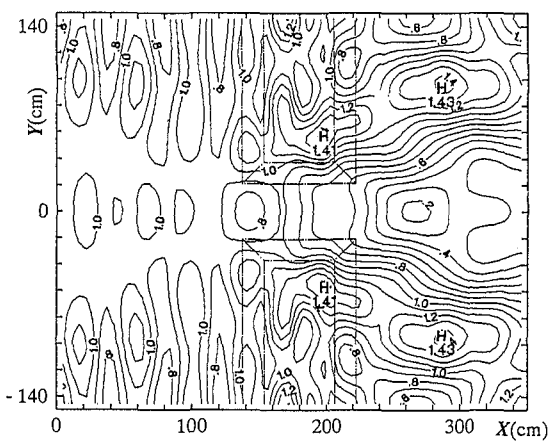

Fig.12 Normalized wave heights, impermeable submerged breakwater, open sea boundary conditions

with the porous breakwater, we see that the partial standing wave patterns in front of the mounds are now more prominent. On the crown, the crests near

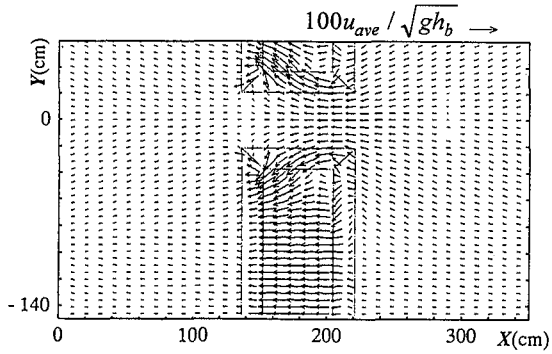

Fig.13 Normalized currents, impermeable submerged breakwater, open sea boundary conditions

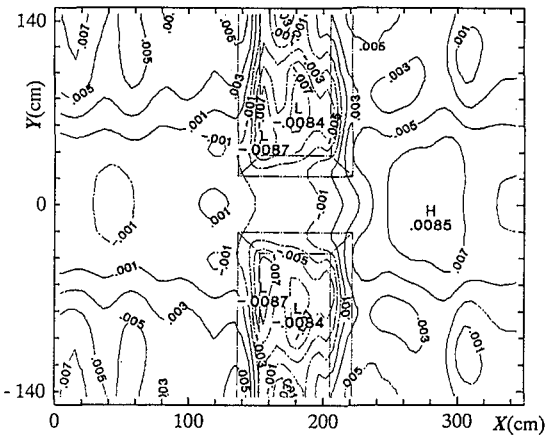

Fig.14 Normalized mean water levels, impermeable submerged breakwater, open sea boundary conditions

the wall are higher and the maximum wave height, although still at the shoreward corner, is higher. The wave heights beyond the gap are likewise higher since the incident wave travels without being damped by the mounds.

The simulated currents are shown in **Fig.13**. Compared with the exterior currents in **Fig.9**, the magnitudes throughout the crown as well as those on either side of the mounds have increased. **Fig.14** shows the corresponding mean water levels. Compared with **Fig.10**, wave set-ups are higher everywhere while setdowns are smaller (in absolute value). On the other hand, the setdown area of the crown has only slightly changed. This suggests that setdown of mean water level on the crown is weakly dependent on porosity.

The difference of the water levels between the inside and outside of areas enclosed by permeable breakwaters depends on a number of variables. Based on the experiments of Diskin et al.[22], the most important of these is the crown submergence relative to the incident wave height. The rise of mean water level in the shoreward side results in an increase of the hydraulic gradient between the inside and outside of the enclosed region. This high gradient has been identified as one of the main causes of movement of bed materials in breakwaters actually constructed on sandy sea beds[22]. Movement of bed material leads to slumping of the structure and is an important consideration in breakwater design. In this aspect, a porous breakwater possesses the structural merit of being less unstable because of its smaller induced hydraulic gradients.

Results of simulations for a higher wave and for shorter periods are reported elsewhere[19]. For the higher wave, the conclusions on the basic characteristics of the normalized nonbreaking wave field are fundamentally similar.

6. CONCLUDING REMARKS

A model for horizontally two-dimensional transformation of nonlinear dispersive waves on arbitrary bottom containing a porous layer is used to study the basic characteristics of the wave and current fields in the vicinity of gaps of submerged breakwaters. Validation of the model with a regular nonbreaking experiment on a wave basin is presented.

Simulation of the wave field around porous and impermeable submerged breakwaters under an open sea condition indicates the following characteristics: (1) The wave field on the seaward side is a coexistence region of waves reflected by the breakwater faces and the oblique waves induced by the gap. (2) Behind the structure, diffraction leads to the existence of a low wave height region behind the gap. (3) The maximum wave height and maximum exterior velocity occur on the breakwater crown around the shoreward corner while the currents are largest on the crown close to the seaward corner. (4) When the breakwater is porous, the exterior currents in the gap vicinity are reduced leading to smaller rises in mean water levels shoreward. A phase lag of horizontal velocities in the exterior and interior of the breakwater indicates the existence of return flow through the porous body. This causes a reduction in extremal velocities on the crown.

It is recognized that scale effects are inevitable when performing experiments involving porous media. For application to field conditions, a proper determination of the porous resistance coefficients, and possibly the inertial coefficient, is necessary. This is possible only through large-scale experiments. Van Gent[23], for example, reported results for rock samples as large as 7.6 cm and proposed a resistance equation in the form of Eqs.(4) and (5) with the coefficients dependent on the transient flow regime.

REFERENCES

1) Dick, T.M. and Brebner, A.: Solid and permeable breakwaters, *Proc., 6th Int. Conf. Coastal Eng., ASCE*, 1141-1158, 1968.
2) Hom-ma, M. and Horikawa, K.: A study on submerged breakwaters, *Coastal Eng. in Japan, JSCE*, Vol.4, 85-102, 1961.
3) Adams, C.B. and Sonu, C.J.: Wave transmission across submerged near-surface breakwaters, *Proc., 20th Int. Conf. Coastal Eng., ASCE*, 1729-1736, 1986.
4) Ijima, T., Eguchi, Y. and Kobayashi, A.: Analysis of wave dissipation by permeable coastal structures (in Japanese), *Proc., 18th Coastal Eng. Conf., JSCE*, 121-130, 1971.
5) Sollitt, C.K. and Cross, R.H.: Wave transmission through permeable breakwater, *Proc., 13th Int. Conf. Coastal Eng., ASCE*, 1827-1846, 1972.
6) Madsen, O.S.: Wave transmission through porous structures, *J. Waterway, Port, Coastal and Ocean Eng., ASCE*, Vol.100, No.WW3, 169-188, 1974.
7) Madsen, P.A.: Wave reflection from a vertical permeable wave absorber, *Coastal Eng.*, 7, 381-396, 1983.
8) Ward, J.C.: Turbulent flow in porous media, *J. Hydraulics Div., ASCE*, Vol.90, No.HY5, 4019-4030, 1964.
9) Sawaragi, T. and Deguchi, I.: Waves on permeable layers, *Proc., 23rd Int. Conf. Coastal Eng., ASCE*, 1531-1544, 1992.
10) Gu, Z. and Wang, H.: Gravity waves over porous bottoms. *Coastal Eng.*, 15, 497-524, 1991.
11) Rojanakamthorn, S., Isobe, M. and Watanabe, A.: Modelling of wave transformation on submerged breakwater, *Proc., 22nd Int. Conf. Coastal Eng., ASCE*, 1060-1073, 1990.
12) Sakakiyama, T. and Kajima, R.: Numerical simulation of nonlinear wave interacting with permeable breakwaters, *Proc., 23rd Int. Conf. Coastal Eng., ASCE*, 1517-1530, 1992.
13) Wibbeler, H. and Oumeraci, H.: Finite element simulation of wave-induced internal flow in rubble mound structures, *Proc., 23rd Int. Conf. Coastal Eng., ASCE*, 1707-1719, 1992.
14) Gu, G.Z. and Wang, H.: Numerical modeling for wave energy dissipation within porous submerged breakwaters of irregular cross section, *Proc., 23rd Int. Conf. Coastal Eng., ASCE*, 1189-1199, 1992.
15) Isobe, M., Shiba, K., Cruz, E.C. and Watanabe, A.: On the nonlinear deformation of waves due to submerged permeable breakwaters (in Japanese), *Proc., Coastal Eng., JSCE*, Vol.38(1), 551-555, 1991.
16) Kioka, W., Kai, H. and Hiraoka, S.: Nonlinear shallow water waves over a porous structure (in Japanese), *Proc., Coastal Eng., JSCE*, Vol.41(2), 711-715, 1994.
17) Van Gent, M.R.A.: The modelling of action on and in coastal structures, *Coastal Eng.*, 24, 311-339, 1994.
18) Cruz, E.C., Isobe, M. and Watanabe, A.: Boussinesq equations for wave transformation on porous beds, *Coastal Engineering*, Vol.30, 125-156, 1997.
19) Cruz, E.C.: Study on submerged breakwaters as wave protection device. *Proc., Symposium on Geotechnical and Coastal Eng.*, Univ. of the Philippines, Session 9: 1-9, 1996.
20) Goda, Y. and Suzuki, Y.: Estimation of incident and reflected waves in random wave experiments, *Proc., 15th Int. Conf. Coastal Eng., ASCE*, 828-845, 1976.
21) Cruz, E.C. and Isobe, M.: Numerical wave absorbers for short and long wave modelling, *Proc., Int. Symp. Waves - Phys. and Num. Modelling, Univ. of British Columbia*, Vol.2, 992-1001, 1994.
22) Diskin, M.H., Vajda, M.L. and Amir, I.: Piling-up behind low and submerged permeable breakwaters. *J. Waterways and Harbors Div., ASCE*, 359-372, 1972.
23) Van Gent, M.R.A.: Porous flow through rubble-mound material, *J. Waterway, Port, Coastal and Ocean Eng., ASCE*, Vol.121, No.3, 176-181, 1995.

(Received May 27, 1996)

平面的に不連続な幅広透過潜堤による波と流れの変形

クルーズ エリック C.・青野利夫

非線形分散波理論にづく数値モデルを用いて，幅広透過潜堤周辺の波浪場と流速場の変形解析を行った．平面水槽を用いた透過潜堤の実験を行い，モデルの妥当性を確認した．数値計算から潜堤を通過する波は，潜堤の天端及び不連続部背後面において極大値をとることが明らかとなった．また，流れは天端面端部の周りで増大し，平均水位の分布がその推進力となっていることが確認された．これらの特性に関して，潜堤の空隙特性との関係が検討された．